Proceedings of FEDSM'03
4TH ASME_JSME Joint Fluids Engineering Conference
Honolulu, Hawaii USA, July 6-11, 2003

FEDSM2003-45812

THE ROLE OF CFD IN PRELIMINARY AEROSPACE DESIGN

Antony Jameson
Department of Aeronautics and Astronautics
Stanford University
jameson@baboon.stanford.edu

Abstract

This paper discusses the role that computational fluid dynamics plays in the design of aircraft. An overview of the design process is provided, covering some of the typical decisions that a design team addresses within a multi-disciplinary environment. On a very regular basis trade-offs between disciplines have to be made where a set of conflicting requirements exists. Within an aircraft development project, we focus on the aerodynamic design problem and review how this process has been advanced, first with the improving capabilities of traditional computational fluid dynamics analyses, and then with aerodynamic optimizations based on these increasingly accurate methods.

1 Background

The past 25 years have seen a revolution in the entire engineering design process as computational simulation has come to play an increasingly dominant role. Most notably, computer aided design (CAD) methods have essentially replaced the drawing board as the basic tool for the definition and control of the configuration. Computer visualization techniques enable the designer to verify that no interferences exist between different parts in the layout, and greatly facilitate decisions on the routing of electrical wiring and hydraulic piping.

Similarly, structural analysis is now almost entirely carried out by computational methods, typically finite element methods. Commercially available software systems have been progressively developed and augmented with new features, and can treat the full range of requirements for aeronautical structures, including the analysis of stressed skin into the nonlinear range. Also, they are very carefully validated against a comprehensive suite of test cases before each new release. Hence, engineers place complete confidence in their results. Accordingly, the structural design is routinely committed on the basis of computational analysis, while structural testing is limited to the role of verification that the design truly meets its specified requirements of ultimate strength and fatigue life.

Computational simulation of fluid flow has not yet reached the same level of maturity. While commercial software for the simulation of fluid flow is offered by numerous vendors, aircraft companies continue to make substantial investments in the in-house development of their own methods. At the same time there are major ongoing efforts to develop the science of computational fluid dynamics (CFD) in government research agencies and Universities. This reflects the fact that fluid flow is generally more complex and harder to predict than the behavior of structures. The complexity and range of phenomena that characterize fluid flow is well illustrated in Van Dyke's Album of Fluid Motion [1].

The concept of a numerical wind tunnel, which might eventually allow computers "to supplant wind tunnels in the aerodynamic design and testing process", was already a topic of discussion in the 1970-1980. In their celebrated paper of 1975, Chapman, Mark and Pirtle [2] listed three main objective of computational aerodynamics:

1. To provide flow simulations that are either impractical or impossible to obtain in wind tunnels or other ground based

experimental test facilities.

2. To lower the time and cost required to obtain aerodynamic flow simulations necessary for the design of new aerospace vehicles.

3. Eventually, to provide more accurate simulations of flight aerodynamics than wind tunnels can.

There have been major advances towards these goals. Despite these, CFD is still not being exploited as effectively as one would like in the design process. This is partially due to the long set-up times and high costs, both human and computational, associated with complex flow simulations. This paper examines ways to exploit computational simulation more effectively in the overall design process, with the primary focus on aerodynamic design, while recognizing that this should be part of an integrated multi-disciplinary process.

The emphasis is on the second of the original goals for a numerical wind tunnel, but also on taking computational methods a step further, to use them not only to predict the aerodynamic properties, but also to find superior designs. The key idea is to embed both analysis and optimization methods in the design process, drawing from both CFD and control theory.

Design trade-offs and the design process itself are surveyed in the next sections. Section 4 discusses the state of the art for CFD in applied aerodynamics, in particular the accuracy of drag prediction. Sections 5-8 examine the way in which optimization techniques can be integrated with CFD. The paper concludes with case studies which apply aerodynamic shape optimization methods within the design process.

2 Aerodynamic Design Tradeoffs

Focusing on the design of long range transport aircraft, a good first estimate of performance is provided by the Breguet range equation:

$$Range = \frac{VL}{D}\frac{1}{SFC}log\frac{W_0+W_f}{W_0}. \tag{1}$$

Here V is the speed, L/D is the lift to drag ratio, SFC is the specific fuel consumption of the engines, W_0 is the loading weight(empty weight + payload+ fuel resourced), and W_f is the weight of fuel burnt.

Equation (1) already displays the multi-disciplinary nature of design. A light weight structure is needed to reduce W_0. The specific fuel consumption is mainly the province of the engine manufacturers, and in fact the largest advances in the last 30 years have been in engine efficiency. The aerodynamic designer should try to maximize VL/D, but must consider the impact of shape modifications on structure weight.

The drag coefficient can be split into an approximately fixed component C_{D_0}, and the induced drag due to lift as

$$C_D = C_{D_0} + \frac{C_L^2}{\pi\varepsilon AR} \tag{2}$$

where AR is the aspect ratio, and ε is an efficiency factor close to unity. C_{D_0} includes contributions such as friction and form drag. It can be seen from this equation that L/D is maximized by flying at a lift coefficient such that the two terms are equal, so that the induced drag is half the total drag. Moreover, the actual drag due to lift

$$D_v = \frac{2L^2}{\pi\varepsilon\rho V^2 b^2}$$

varies inversely with the square of the span b. Thus there is a direct conflict between reducing the drag by increasing the span and reducing the structure weight by decreasing it.

It also follows from equation (1) that one should try to maximize VL/D. This means that the cruising speed V should be increased until it approaches the speed of sound C, at which point the formation of shock waves causes the onset of "drag-rise" . Typically the lift to drag ratio will drop from around 19 at a Mach number V/C in the neighborhood of 0.85, to the order of 4 at Mach 1. Thus the optimum cruise speed will be in the transonic regime, when shock waves are beginning to form , but remain weak enough only to incur a small drag penalty.

The designer can reduce shock drag and delay the onset of drag-rise by increasing the sweep back of the wing or reducing its thickness. Increasing the sweepback increases the structure weight, and may incur problems with stability and control. Decreasing the thickness both reduces the fuel volume (since the wing is used as the main fuel tank), and increases the structure weight, because for a given stress level in the skin and a given skin thickness, the bending moment that can be supported is directly proportional to the depth of the wing. In the absence of winglets, the optimum span load distribution is elliptic, giving an efficiency factor $\varepsilon = 1$. When, however, the structure weight is taken into account, it is better to shift the load distribution inboard in order to reduce the root bending moment. It may also be necessary to limit the section lift coefficient in the outboard part of the wing in order to delay the onset of buffet, which may occur when the lift coefficient is increased to make a turn at a high Mach number.

3 Design Process

The design process can generally be divided into three phases: conceptual design, preliminary design, and final detailed design, as illustrated in Figure 1.

The conceptual design stage defines the mission in the light of anticipated market requirements, and determines a general preliminary configuration capable of performing this mission, together with first estimates of size, weight and performance. A conceptual design requires a staff of 15-30 people. Over a period of 1-2 years, the initial business case is developed. The costs of this phase are the range of 6-12 million dollars, and there is minimal airline involvement

In the preliminary design stage the aerodynamic shape and structural skeleton progress to the point where detailed performance estimates can be made and guaranteed to potential customers, who can then, in turn, formally sign binding contracts for the purchase of a certain number of aircraft. At this stage the development costs are still fairly moderate. A staff of 100-300 people is generally employed for up to 2 years, at a cost of 60-120 million dollars. Initial aerodynamic performance is explored through wind tunnel tests.

In the final design stage the structure must be defined in complete detail, together with complete systems, including the flight deck, control systems (involving major software development for fly-by-wire systems), avionics, electrical and hydraulic systems, landing gear, weapon systems for military aircraft, and cabin layout for commercial aircraft. Major costs are incurred at this stage, during which it is also necessary to prepare a detailed manufacturing plan, together with appropriate facilities and tooling. A staff of thousands of people define every part of the aircraft. Wind Tunnel validation of the final design is carried out. Significant development costs are incurred over a 3 year period, plus an additional year of Flight Testing and Structural Qualification Testing for Certification. Total costs are in the range of 3-12 billion dollars. Thus, the final design would normally be carried out only if sufficient orders have been received to indicate a reasonably high probability of recovering a significant fraction of the investment. For a commercial aircraft there are extensive discussions with airlines.

In the development of commercial aircraft, aerodynamic design plays a leading role during the preliminary design stage, during which the definition of the external aerodynamic shape is typically finalized. The aerodynamic lines of the Boeing 777 were frozen, for example, when initial orders were accepted before the initiation of the detailed design of the structure. Figure 2 illustrates the way in which the aerodynamic design process is embedded in the overall preliminary design. The starting point is an initial CAD definition resulting from the conceptual design. The inner loop of aerodynamic analysis is contained in an outer multi-disciplinary loop, which is in turn contained in a major design cycle involving wind tunnel testing. In recent Boeing practice, three major design cycles, each requiring about 4-6 months, have been used to finalize the wing design. Improvements in CFD which would allow the elimination of a major cycle would significantly shorten the overall design process and therefore reduce costs.

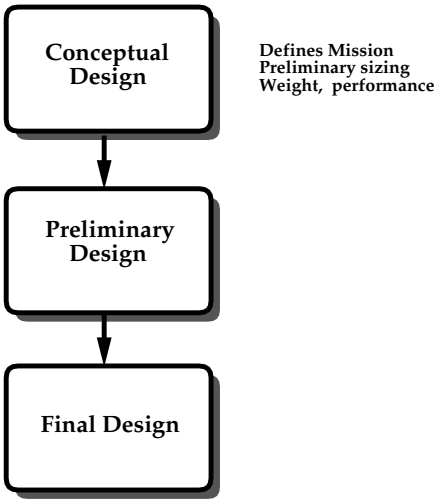

Figure 1. The Overall Design Process

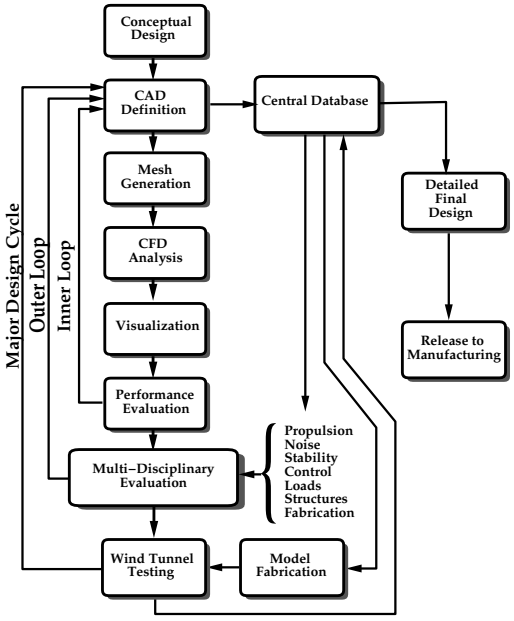

Figure 2. The Aerodynamic Design Process

The inner aerodynamic design loop is used to evaluate numerous variations in the wing definition. In each iteration it is necessary to generate a mesh for the new configuration prior to performing the CFD analysis. Computer graphics software is then used to visualize the results, and the performance is evaluated. The first studies may be confined to partial configurations

such as wing-body or wing-body-nacelle combinations. At this stage the focus is on the design of the clean wing. Key points of the flight envelope include the nominal cruise point, cruise at high lift and low lift to allow for the weight variation between the initial and final cruise as the fuel is burned off, and a long range cruise point at lower Mach number, where it is important to ensure there is no significant drag creep. Other defining points are the climb condition, which requires a good lift to drag ratio at low Mach number and high lift coefficient for the clean wing, and buffet conditions. The buffet requirement is typically taken as the high lift cruise point increased to a load of 1.3 g to allow for maneuvering and gust loads.

The aerodynamic analysis interacts with the other disciplines in the next outer loop. These disciplines have their own inner loops, not shown in Figure 2. For an efficient design process the fully updated aero-design database must be accessible to other disciplines without loss of information. For example, the thrust requirements for the power plant design will depend on the drag estimates for take-off, climb and cruise. In order to meet airport noise constraints a rapid climb may be required while the thrust may also be limited. Initial estimates of the lift and moments allow preliminary sizing of the horizontal and vertical tail. This interacts with the design of the control system, where the use of a fly-by-wire system may allow relaxed static stability, hence tail surfaces of reduced size.

First estimates of the aerodynamic loads allow the design of an initial structural skeleton, which in turn provides a weight estimate of the structure. One of the main trade-offs is between aerodynamic performance and wing structure weight. The requirement for fuel volume may also be an important consideration. Manufacturing constraints must also be considered in the final definition of the aerodynamic shape. For example, the curvature in the spanwise direction should be limited. This avoids the need for shot peening which might otherwise be required to produce curvature in both the spanwise and chordwise directions.

From the foregoing considerations, it is apparent that in order to carry out the inner loop of the aerodynamic design process the main requirements for effective CFD software are:

1. Sufficient and known level of accuracy
2. Acceptable computational and manpower costs
3. Fast turn around time

4 Performance Prediction

The discussion in section 2 illustrates how performance estimation at the cruise condition is crucial to the design of long-range transport aircraft. The error should be on the order of 1 percent or less. The drag coefficient of a typical transport aircraft, such as the Boeing 747, is about 0.0275 (275 counts) for a typical lift coefficient of approximately 0.5. The drag coefficient of proposed supersonic transport designs is in the range of 0.0120 to 0.0150 at much lower lift coefficients in the range of 0.1 to 0.12. Thus one should aim to predict drag with an accuracy of 1 to 2 counts. Manufacturers have to guarantee performance, and errors can be very expensive due to the costs of redesign, penalty payments and lost orders.

In order to achieve this level of accuracy, it is ultimately essential to use the Reynolds-Averaged Navier-Stokes (RANS) equations. However, to accelerate their initial efforts, designers typically use CFD methods based on less sophisticated flow models, such as the full-potential or Euler equations coupled with a boundary-layer method. In order to allow the completion of the major design cycle in 4-6 months, the cycle time for the multidisciplinary loop should not be greater than about 2 weeks. Considering the need to examine the performance of design variations at all the key points of the flight envelope, this implies the need to turn around aerodynamic analysis in a few hours. The computational costs are also important because the cumulative costs of large numbers of calculations can become a limiting factor.

The state-of-the-art in CFD drag prediction was recently assessed by an international workshop on the subject. A summary of the results of the workshop is presented in Reference [3]. Figure 4 provides the 28 drag polars resulting from this drag prediction workshop (DPW). Also included in this figure are the available test data [4] for the DLR-F4 wing/body configuration, which was the subject of the study. With the exception of a few out-layers, the computed polars fall within a band of about $\pm 7\%$ the absolute level. The slopes, $\frac{dC_L^2}{dC_D}$, are nearly identical. When comparing the CFD results with the test data, we note that the CFD solutions were all run assuming fully-turbulent flow, while the test data were collected with laminar runs on the wing up to transition strips on both upper and lower surfaces. To quantify the shift in drag associated with this difference, several independent calculations were performed yielding 12-13 counts higher drag levels for the fully-turbulent flows. Accounting for this adjustment, the center of the CFD drag polars band coincides with the mean of the test polars. While this indicates that the industry as a whole is closing in on the ability to compute accurate absolute drag levels, in general, the errors are not to the level desired by aircraft design teams. However, a few of the results submitted to the DPW fall within the uncertainty band of the experimental data. For example, the corresponding results of Reference [5] are shown in Figure 5. Achieving this level of accuracy is dominated by the quality of the underlying grid, but also depends on the turbulence model, the level of convergence, discretization scheme, etc. It is imperative that each of these areas be studied independently of each other, otherwise "accurate" results might be obtained as a consequence of cancellation of errors. Unfortunately, an optimization based on an analysis method containing such a cancellation of errors will most likely emphasize its weakness and probably yield a new design with a false performance improvement.

5 Aerodynamic Shape Optimization

Traditionally the process of selecting design variations has been carried out by trial and error, relying on the intuition and experience of the designer. It is also evident that the number of possible design variations is too large to permit their exhaustive evaluation, and thus it is very unlikely that a truly optimum solution can be found without the assistance of automatic optimization procedures. In order to take full advantage of the possibility of examining a large design space, the numerical simulations need to be combined with automatic search and optimization procedures. This can lead to automatic design methods which will fully realize the potential improvements in aerodynamic efficiency.

Ultimately there is a need for multi-disciplinary optimization (MDO), but this can only be effective if it is based on sufficiently high fidelity modeling of the separate disciplines. As a step in this direction there could be significant pay-offs from the application of optimization techniques within the disciplines, where the interactions with other disciplines are taken into account through the introduction of constraints. For example the wing drag can be minimized at a given Mach number and lift coefficient with a fixed planform, and constraints on minimum thickness to meet requirements for fuel volume and structure weight.

An approach which has become increasingly popular is to carry out a search over a large number of variations via a genetic algorithm. This may allow the discovery of (sometimes unexpected) optimum design choices in very complex multi-objective problems, but it becomes extremely expensive when each evaluation of the cost function requires intensive computation, as is the case in aerodynamic problems.

In order to find optimum aerodynamic shapes with reasonable computational costs, it pays to regard the wing as a device which controls the flow in order to produce lift with minimum drag. As a result, one can draw on concepts which have been developed in the mathematical theory of control of systems governed by partial differential equations. In particular, an acceptable aerodynamic design must have characteristics that smoothly vary with small changes in shape and flow conditions. Consequently, gradient-based procedures are appropriate for aerodynamic shape optimization. Two main issues affect the efficiency of gradient-based procedures; the first is the actual calculation of the gradient, and the second is the construction of an efficient search procedure which utilizes the gradient.

5.1 Gradient Calculation

For the class of aerodynamic optimization problems under consideration, the design space is essentially infinitely dimensional. Suppose that the performance of a system design can be measured by a cost function I which depends on a function $\mathcal{F}(x)$ that describes the shape,where under a variation of the design $\delta\mathcal{F}(x)$, the variation of the cost is δI. Now suppose that δI can be expressed to first order as

$$\delta I = \int \mathcal{G}(x)\delta\mathcal{F}(x)dx$$

where $\mathcal{G}(x)$ is the gradient. Then by setting

$$\delta\mathcal{F}(x) = -\lambda\mathcal{G}(x)$$

one obtains an improvement

$$\delta I = -\lambda\int \mathcal{G}^2(x)dx$$

unless $\mathcal{G}(x) = 0$. Thus the vanishing of the gradient is a necessary condition for a local minimum.

Computing the gradient of a cost function for a complex system can be a numerically intensive task, especially if the number of design parameters is large and the cost function is an expensive evaluation. The simplest approach to optimization is to define the geometry through a set of design parameters, which may, for example, be the weights α_i applied to a set of shape functions $\mathcal{B}_i(x)$ so that the shape is represented as

$$\mathcal{F}(x) = \sum \alpha_i\mathcal{B}_i(x).$$

Then a cost function I is selected which might be the drag coefficient or the lift to drag ratio; I is regarded as a function of the parameters α_i. The sensitivities $\frac{\partial I}{\partial\alpha_i}$ may now be estimated by making a small variation $\delta\alpha_i$ in each design parameter in turn and recalculating the flow to obtain the change in I. Then

$$\frac{\partial I}{\partial\alpha_i} \approx \frac{I(\alpha_i+\delta\alpha_i) - I(\alpha_i)}{\delta\alpha_i}.$$

The main disadvantage of this finite-difference approach is that the number of flow calculations needed to estimate the gradient is proportional to the number of design variables [6]. Similarly, if one resorts to direct code differentiation (ADIFOR [7,8]), or complex-variable perturbations [9], the cost of determining the gradient is also directly proportional to the number of variables used to define the design.

A more cost effective technique is to compute the gradient through the solution of an adjoint problem, such as that developed in references [10–12]. The essential idea may be summarized as follows. For flow about an arbitrary body, the aerodynamic properties that define the cost function are functions of

the flowfield variables (w) and the physical shape of the body, which may be represented by the function $\mathcal{F}$. Then

$$I = I(w, \mathcal{F})$$

and a change in $\mathcal{F}$ results in a change of the cost function

$$\delta I = \frac{\partial I^T}{\partial w}\delta w + \frac{\partial I^T}{\partial \mathcal{F}}\delta \mathcal{F}.$$

Using a technique drawn from control theory, the governing equations of the flowfield are introduced as a constraint in such a way that the final expression for the gradient does not require reevaluation of the flowfield. In order to achieve this, δw must be eliminated from the above equation. Suppose that the governing equation R, which expresses the dependence of w and $\mathcal{F}$ within the flowfield domain D, can be written as

$$R(w, \mathcal{F}) = 0. \tag{3}$$

Then δw is determined from the equation

$$\delta R = \left[\frac{\partial R}{\partial w}\right]\delta w + \left[\frac{\partial R}{\partial \mathcal{F}}\right]\delta \mathcal{F} = 0.$$

Next, introducing a Lagrange multiplier ψ, we have

$$\delta I = \frac{\partial I^T}{\partial w}\delta w + \frac{\partial I^T}{\partial \mathcal{F}}\delta \mathcal{F} - \psi^T\left(\left[\frac{\partial R}{\partial w}\right]\delta w + \left[\frac{\partial R}{\partial \mathcal{F}}\right]\delta \mathcal{F}\right). \tag{4}$$

With some rearrangement

$$\delta I = \left(\frac{\partial I^T}{\partial w} - \psi^T\left[\frac{\partial R}{\partial w}\right]\right)\delta w + \left(\frac{\partial I^T}{\partial \mathcal{F}} - \psi^T\left[\frac{\partial R}{\partial \mathcal{F}}\right]\right)\delta \mathcal{F}.$$

Choosing ψ to satisfy the adjoint equation

$$\left[\frac{\partial R}{\partial w}\right]^T \psi = \frac{\partial I^T}{\partial w} \tag{5}$$

the term multiplying δw can be eliminated in the variation of the cost function, and we find that

$$\delta I = \mathcal{G}\delta \mathcal{F},$$

where

$$\mathcal{G} = \frac{\partial I^T}{\partial \mathcal{F}} - \psi^T\left[\frac{\partial R}{\partial \mathcal{F}}\right].$$

The advantage is that the variation in cost function is independent of δw, with the result that the gradient of I with respect to any number of design variables can be determined without the need for additional flow-field evaluations.

In the case that (3) is a partial differential equation, the adjoint equation (5) is also a partial differential equation and appropriate boundary conditions must be determined. It turns out that the appropriate boundary conditions depend on the choice of the cost function, and may easily be derived for cost functions that involve surface-pressure integrations. Cost functions involving field integrals lead to the appearance of a source term in the adjoint equation.

The cost of solving the adjoint equation is comparable to that of solving the flow equation. Hence, the cost of obtaining the gradient is comparable to the cost of two function evaluations, regardless of the dimension of the design space.

6 Design using the Euler Equations

The application of control theory to aerodynamic design problems is illustrated in this section for the case of three-dimensional wing design using the compressible Euler equations as the mathematical model. The extension of the method to treat the Navier-Stokes equations is presented in references [13–15]. It proves convenient to denote the Cartesian coordinates and velocity components by x_1, x_2, x_3 and u_1, u_2, u_3, and to use the convention that summation over $i = 1$ to 3 is implied by a repeated index i. Then, the three-dimensional Euler equations may be written as

$$\frac{\partial w}{\partial t} + \frac{\partial f_i}{\partial x_i} = 0 \quad \text{in } D, \tag{6}$$

where

$$w = \begin{Bmatrix} \rho \\ \rho u_1 \\ \rho u_2 \\ \rho u_3 \\ \rho E \end{Bmatrix}, \quad f_i = \begin{Bmatrix} \rho u_i \\ \rho u_i u_1 + p\delta_{i1} \\ \rho u_i u_2 + p\delta_{i2} \\ \rho u_i u_3 + p\delta_{i3} \\ \rho u_i H \end{Bmatrix} \tag{7}$$

and δ_{ij} is the Kronecker delta function. Also,

$$p = (\gamma - 1)\rho\left\{E - \frac{1}{2}\left(u_i^2\right)\right\}, \tag{8}$$

and

$$\rho H = \rho E + p \tag{9}$$

where γ is the ratio of the specific heats.

In order to simplify the derivation of the adjoint equations, we map the solution to a fixed computational domain with coordinates ξ_1, ξ_2, ξ_3 where

$$K_{ij} = \left[\frac{\partial x_i}{\partial \xi_j}\right], \; J = \det(K), \; K^{-1}_{ij} = \left[\frac{\partial \xi_i}{\partial x_j}\right],$$

and

$$S = JK^{-1}.$$

The elements of S are the cofactors of K, and in a finite volume discretization they are just the face areas of the computational cells projected in the x_1, x_2, and x_3 directions. Using the permutation tensor ε_{ijk} we can express the elements of S as

$$S_{ij} = \frac{1}{2}\varepsilon_{jpq}\varepsilon_{irs}\frac{\partial x_p}{\partial \xi_r}\frac{\partial x_q}{\partial \xi_s}. \tag{10}$$

Then

$$\begin{aligned}\frac{\partial}{\partial \xi_i}S_{ij} &= \frac{1}{2}\varepsilon_{jpq}\varepsilon_{irs}\left(\frac{\partial^2 x_p}{\partial \xi_r \partial \xi_i}\frac{\partial x_q}{\partial \xi_s} + \frac{\partial x_p}{\partial \xi_r}\frac{\partial^2 x_q}{\partial \xi_s \partial \xi_i}\right)\\ &= 0.\end{aligned} \tag{11}$$

Also in the subsequent analysis of the effect of a shape variation it is useful to note that

$$\begin{aligned}S_{1j} &= \varepsilon_{jpq}\frac{\partial x_p}{\partial \xi_2}\frac{\partial x_q}{\partial \xi_3},\\ S_{2j} &= \varepsilon_{jpq}\frac{\partial x_p}{\partial \xi_3}\frac{\partial x_q}{\partial \xi_1},\\ S_{3j} &= \varepsilon_{jpq}\frac{\partial x_p}{\partial \xi_1}\frac{\partial x_q}{\partial \xi_2}.\end{aligned} \tag{12}$$

Now, multiplying equation(6) by J and applying the chain rule,

$$J\frac{\partial w}{\partial t} + R(w) = 0 \tag{13}$$

where

$$R(w) = S_{ij}\frac{\partial f_j}{\partial \xi_i} = \frac{\partial}{\partial \xi_i}(S_{ij}f_j), \tag{14}$$

using (11). We can write the transformed fluxes in terms of the scaled contravariant velocity components

$$U_i = S_{ij}u_j$$

as

$$F_i = S_{ij}f_j = \begin{bmatrix}\rho U_i\\ \rho U_i u_1 + S_{i1}p\\ \rho U_i u_2 + S_{i2}p\\ \rho U_i u_3 + S_{i3}p\\ \rho U_i H\end{bmatrix}.$$

For convenience, the coordinates ξ_i describing the fixed computational domain are chosen so that each boundary conforms to a constant value of one of these coordinates. Variations in the shape then result in corresponding variations in the mapping derivatives defined by K_{ij}. Suppose that the performance is measured by a cost function

$$I = \int_{\mathcal{B}} \mathcal{M}(w,S)\, dB_\xi + \int_{\mathcal{D}} \mathcal{P}(w,S)\, dD_\xi,$$

containing both boundary and field contributions where dB_ξ and dD_ξ are the surface and volume elements in the computational domain. In general, $\mathcal{M}$ and $\mathcal{P}$ will depend on both the flow variables w and the metrics S defining the computational space. The design problem is now treated as a control problem where the boundary shape represents the control function, which is chosen to minimize I subject to the constraints defined by the flow equations (13). A shape change produces a variation in the flow solution δw and the metrics δS which in turn produce a variation in the cost function

$$\delta I = \int_{\mathcal{B}} \delta\mathcal{M}(w,S)\, dB_\xi + \int_{\mathcal{D}} \delta\mathcal{P}(w,S)\, dD_\xi. \tag{15}$$

This can be split as

$$\delta I = \delta I_I + \delta I_{II}, \tag{16}$$

with

$$\begin{aligned}\delta\mathcal{M} &= [\mathcal{M}_w]_I\,\delta w + \delta\mathcal{M}_{II},\\ \delta\mathcal{P} &= [\mathcal{P}_w]_I\,\delta w + \delta\mathcal{P}_{II},\end{aligned} \tag{17}$$

where we continue to use the subscripts I and II to distinguish between the contributions associated with the variation of the flow solution δw and those associated with the metric variations δS. Thus $[\mathcal{M}_w]_I$ and $[\mathcal{P}_w]_I$ represent $\frac{\partial \mathcal{M}}{\partial w}$ and $\frac{\partial \mathcal{P}}{\partial w}$ with the metrics fixed, while $\delta\mathcal{M}_{II}$ and $\delta\mathcal{P}_{II}$ represent the contribution of the metric variations δS to $\delta\mathcal{M}$ and $\delta\mathcal{P}$.

In the steady state, the constraint equation (13) specifies the variation of the state vector δw by

$$\delta R = \frac{\partial}{\partial \xi_i} \delta F_i = 0. \tag{18}$$

Here also, δR and δF_i can be split into contributions associated with δw and δS using the notation

$$\begin{aligned} \delta R &= \delta R_I + \delta R_{II} \\ \delta F_i &= [F_{iw}]_I \, \delta w + \delta F_{iII}. \end{aligned} \tag{19}$$

where

$$[F_{iw}]_I = S_{ij} \frac{\partial f_i}{\partial w}.$$

Multiplying by a co-state vector ψ, which will play an analogous role to the Lagrange multiplier introduced in equation (4), and integrating over the domain produces

$$\int_{\mathcal{D}} \psi^T \frac{\partial}{\partial \xi_i} \delta F_i d\mathcal{D}_\xi = 0. \tag{20}$$

Assuming that ψ is differentiable, the terms with subscript I may be integrated by parts to give

$$\int_{\mathcal{B}} n_i \psi^T \delta F_{i_I} d\mathcal{B}_\xi - \int_{\mathcal{D}} \frac{\partial \psi^T}{\partial \xi_i} \delta F_{i_I} d\mathcal{D}_\xi + \int_{\mathcal{D}} \psi^T \delta R_{II} d\mathcal{D}_\xi = 0. \tag{21}$$

This equation results directly from taking the variation of the weak form of the flow equations, where ψ is taken to be an arbitrary differentiable test function. Since the left hand expression equals zero, it may be subtracted from the variation in the cost function (15) to give

$$\begin{aligned} \delta I = \delta I_{II} &- \int_{\mathcal{D}} \psi^T \delta R_{II} d\mathcal{D}_\xi - \int_{\mathcal{B}} \left[\delta \mathcal{M}_I - n_i \psi^T \delta F_{i_I} \right] d\mathcal{B}_\xi \\ &+ \int_{\mathcal{D}} \left[\delta \mathcal{P}_I + \frac{\partial \psi^T}{\partial \xi_i} \delta F_{i_I} \right] d\mathcal{D}_\xi. \end{aligned} \tag{22}$$

Now, since ψ is an arbitrary differentiable function, it may be chosen in such a way that δI no longer depends explicitly on the variation of the state vector δw. The gradient of the cost function can then be evaluated directly from the metric variations without having to recompute the variation δw resulting from the perturbation of each design variable.

Comparing equations (17) and (19), the variation δw may be eliminated from (22) by equating all field terms with subscript "I" to produce a differential adjoint system governing ψ

$$\frac{\partial \psi^T}{\partial \xi_i} [F_{iw}]_I + [\mathcal{P}_w]_I = 0 \quad \text{in } \mathcal{D}. \tag{23}$$

Taking the transpose of equation (23), in the case that there is no field integral in the cost function, the inviscid adjoint equation may be written as

$$C_i^T \frac{\partial \psi}{\partial \xi_i} = 0 \quad \text{in } \mathcal{D}, \tag{24}$$

where the inviscid Jacobian matrices in the transformed space are given by

$$C_i = S_{ij} \frac{\partial f_j}{\partial w}.$$

The corresponding adjoint boundary condition is produced by equating the subscript "I" boundary terms in equation (22) to produce

$$n_i \psi^T [F_{iw}]_I = [\mathcal{M}_w]_I \quad \text{on } \mathcal{B}. \tag{25}$$

The remaining terms from equation (22) then yield a simplified expression for the variation of the cost function which defines the gradient

$$\delta I = \delta I_{II} + \int_{\mathcal{D}} \psi^T \delta R_{II} d\mathcal{D}_\xi, \tag{26}$$

which consists purely of the terms containing variations in the metrics, with the flow solution fixed. Hence an explicit formula for the gradient can be derived once the relationship between mesh perturbations and shape variations is defined.

The details of the formula for the gradient depend on the way in which the boundary shape is parameterized as a function of the design variables, and the way in which the mesh is deformed as the boundary is modified. Using the relationship between the mesh deformation and the surface modification, the field integral is reduced to a surface integral by integrating along the coordinate lines emanating from the surface. Thus the expression for

δI is finally reduced to the form

$$\delta I = \int_{\mathcal{B}} \mathcal{G}\delta\mathcal{F}\, d\mathcal{B}_\xi$$

where $\mathcal{F}$ represents the design variables, and $\mathcal{G}$ is the gradient, which is a function defined over the boundary surface.

The boundary conditions satisfied by the flow equations restrict the form of the left hand side of the adjoint boundary condition (25). Consequently, the boundary contribution to the cost function $\mathcal{M}$ cannot be specified arbitrarily. Instead, it must be chosen from the class of functions which allow cancellation of all terms containing δw in the boundary integral of equation (22). On the other hand, there is no such restriction on the specification of the field contribution to the cost function $\mathcal{P}$, since these terms may always be absorbed into the adjoint field equation (23) as source terms.

For simplicity, it will be assumed that the portion of the boundary that undergoes shape modifications is restricted to the coordinate surface $\xi_2 = 0$. Then equations (22) and (25) may be simplified by incorporating the conditions

$$n_1 = n_3 = 0, \quad n_2 = 1, \quad d\mathcal{B}_\xi = d\xi_1 d\xi_3,$$

so that only the variation δF_2 needs to be considered at the wall boundary. The condition that there is no flow through the wall boundary at $\xi_2 = 0$ is equivalent to

$$U_2 = 0,$$

so that

$$\delta U_2 = 0$$

when the boundary shape is modified. Consequently the variation of the inviscid flux at the boundary reduces to

$$\delta F_2 = \delta p \begin{Bmatrix} 0 \\ S_{21} \\ S_{22} \\ S_{23} \\ 0 \end{Bmatrix} + p \begin{Bmatrix} 0 \\ \delta S_{21} \\ \delta S_{22} \\ \delta S_{23} \\ 0 \end{Bmatrix}. \tag{27}$$

Since δF_2 depends only on the pressure, it is now clear that the performance measure on the boundary $\mathcal{M}(w,S)$ may only be a function of the pressure and metric terms. Otherwise, complete cancellation of the terms containing δw in the boundary integral would be impossible. One may, for example, include arbitrary measures of the forces and moments in the cost function, since these are functions of the surface pressure.

In order to design a shape which will lead to a desired pressure distribution, a natural choice is to set

$$I = \frac{1}{2}\int_{\mathcal{B}} (p - p_d)^2\, dS$$

where p_d is the desired surface pressure, and the integral is evaluated over the actual surface area. In the computational domain this is transformed to

$$I = \frac{1}{2}\int\int_{\mathcal{B}_w} (p - p_d)^2 |S_2|\, d\xi_1 d\xi_3,$$

where the quantity

$$|S_2| = \sqrt{S_{2j} S_{2j}}$$

denotes the face area corresponding to a unit element of face area in the computational domain. Now, to cancel the dependence of the boundary integral on δp, the adjoint boundary condition reduces to

$$\psi_j n_j = p - p_d \tag{28}$$

where n_j are the components of the surface normal

$$n_j = \frac{S_{2j}}{|S_2|}.$$

This amounts to a transpiration boundary condition on the costate variables corresponding to the momentum components. Note that it imposes no restriction on the tangential component of ψ at the boundary.

We find finally that

$$\delta I = -\int_{\mathcal{D}} \frac{\partial \psi^T}{\partial \xi_i} \delta S_{ij} f_j d\mathcal{D} - \int\int_{B_W} (\delta S_{21}\psi_2 + \delta S_{22}\psi_3 + \delta S_{23}\psi_4)\, p\, d\xi_1 d\xi_3. \tag{29}$$

Here the expression for the cost variation depends on the mesh variations throughout the domain which appear in the field integral. However, the true gradient for a shape variation should not

depend on the way in which the mesh is deformed, but only on the true flow solution. In the next section we show how the field integral can be eliminated to produce a reduced gradient formula which depends only on the boundary movement.

7 The Reduced Gradient Formulation

Consider the case of a mesh variation with a fixed boundary. Then,

$$\delta I = 0$$

but there is a variation in the transformed flux,

$$\delta F_i = C_i \delta w + \delta S_{ij} f_j.$$

Here the true solution is unchanged. Thus, the variation δw is due to the mesh movement δx at each mesh point. Therefore

$$\delta w = \nabla w \cdot \delta x = \frac{\partial w}{\partial x_j} \delta x_j \, (= \delta w^*)$$

and since

$$\frac{\partial}{\partial \xi_i} \delta F_i = 0,$$

it follows that

$$\frac{\partial}{\partial \xi_i} \left(\delta S_{ij} f_j \right) = -\frac{\partial}{\partial \xi_i} \left(C_i \delta w^* \right). \tag{30}$$

It is verified below that this relation holds in the general case with boundary movement. Now

$$\begin{aligned} \int_{\mathcal{D}} \phi^T \delta R d\mathcal{D} &= \int_{\mathcal{D}} \phi^T \frac{\partial}{\partial \xi_i} C_i \left(\delta w - \delta w^* \right) d\mathcal{D} \\ &= \int_{\mathcal{B}} \phi^T C_i \left(\delta w - \delta w^* \right) d\mathcal{B} \\ &- \int_{\mathcal{D}} \frac{\partial \phi^T}{\partial \xi_i} C_i \left(\delta w - \delta w^* \right) d\mathcal{D}. \end{aligned} \tag{31}$$

Here on the wall boundary

$$C_2 \delta w = \delta F_2 - \delta S_{2j} f_j. \tag{32}$$

Thus, by choosing ϕ to satisfy the adjoint equation (24) and the adjoint boundary condition (25), we reduce the cost variation to a boundary integral which depends only on the surface displacement:

$$\begin{aligned} \delta I = &\int_{\mathcal{B}_W} \psi^T \left(\delta S_{2j} f_j + C_2 \delta w^* \right) d\xi_1 d\xi_3 \\ &- \iint_{B_W} \left(\delta S_{21} \psi_2 + \delta S_{22} \psi_3 + \delta S_{23} \psi_4 \right) p \, d\xi_1 d\xi_3. \end{aligned} \tag{33}$$

For completeness the general derivation of equation(30) is presented here. Using the formula(10), and the property (11)

$$\begin{aligned} &\tfrac{\partial}{\partial \xi_i} \left(\delta S_{ij} f_j \right) \\ &= \frac{1}{2} \frac{\partial}{\partial \xi_i} \left\{ \varepsilon_{jpq} \varepsilon_{irs} \left(\frac{\partial \delta x_p}{\partial \xi_r} \frac{\partial x_q}{\partial \xi_s} + \frac{\partial x_p}{\partial \xi_r} \frac{\partial \delta x_q}{\partial \xi_s} \right) f_j \right\} \\ &= \frac{1}{2} \varepsilon_{jpq} \varepsilon_{irs} \left(\frac{\partial \delta x_p}{\partial \xi_r} \frac{\partial x_q}{\partial \xi_s} + \frac{\partial x_p}{\partial \xi_r} \frac{\partial \delta x_q}{\partial \xi_s} \right) \frac{\partial f_j}{\partial \xi_i} \\ &= \frac{1}{2} \varepsilon_{jpq} \varepsilon_{irs} \left\{ \frac{\partial}{\partial \xi_r} \left(\delta x_p \frac{\partial x_q}{\partial \xi_s} \frac{\partial f_j}{\partial \xi_i} \right) \right\} \\ &+ \frac{1}{2} \varepsilon_{jpq} \varepsilon_{irs} \left\{ \frac{\partial}{\partial \xi_s} \left(\delta x_q \frac{\partial x_p}{\partial \xi_r} \frac{\partial f_j}{\partial \xi_i} \right) \right\} \\ &= \frac{\partial}{\partial \xi_r} \left(\delta x_p \varepsilon_{pqj} \varepsilon_{rsi} \frac{\partial x_q}{\partial \xi_s} \frac{\partial f_j}{\partial \xi_i} \right). \end{aligned} \tag{34}$$

Now express δx_p in terms of a shift in the original computational coordinates

$$\delta x_p = \frac{\partial x_p}{\partial \xi_k} \delta \xi_k.$$

Then we obtain

$$\frac{\partial}{\partial \xi_i} \left(\delta S_{ij} f_j \right) = \frac{\partial}{\partial \xi_r} \left(\varepsilon_{pqj} \varepsilon_{rsi} \frac{\partial x_p}{\partial \xi_k} \frac{\partial x_q}{\partial \xi_s} \frac{\partial f_j}{\partial \xi_i} \delta \xi_k \right). \tag{35}$$

The term in $\frac{\partial}{\partial \xi_1}$ is

$$\varepsilon_{123} \varepsilon_{pqj} \frac{\partial x_p}{\partial \xi_k} \left(\frac{\partial x_q}{\partial \xi_2} \frac{\partial f_j}{\partial \xi_3} - \frac{\partial x_q}{\partial \xi_3} \frac{\partial f_j}{\partial \xi_2} \right) \delta \xi_k.$$

Here the term multiplying $\delta \xi_1$ is

$$\varepsilon_{jpq} \left(\frac{\partial x_p}{\partial \xi_1} \frac{\partial x_q}{\partial \xi_2} \frac{\partial f_j}{\partial \xi_3} - \frac{\partial x_p}{\partial \xi_1} \frac{\partial x_q}{\partial \xi_3} \frac{\partial f_j}{\partial \xi_2} \right).$$

According to the formulas(12) this may be recognized as

$$S_{2j}\frac{\partial f_1}{\partial \xi_2}+S_{3j}\frac{\partial f_1}{\partial \xi_3}$$

or, using the quasi-linear form(14) of the equation for steady flow, as

$$-S_{1j}\frac{\partial f_1}{\partial \xi_1}.$$

The terms multiplying $\delta\xi_2$ and $\delta\xi_3$ are

$$\varepsilon_{jpq}\left(\frac{\partial x_p}{\partial \xi_2}\frac{\partial x_q}{\partial \xi_2}\frac{\partial f_j}{\partial \xi_3}-\frac{\partial x_p}{\partial \xi_2}\frac{\partial x_q}{\partial \xi_3}\frac{\partial f_j}{\partial \xi_2}\right)=-S_{1j}\frac{\partial f_1}{\partial \xi_2}$$

and

$$\varepsilon_{jpq}\left(\frac{\partial x_p}{\partial \xi_3}\frac{\partial x_q}{\partial \xi_2}\frac{\partial f_j}{\partial \xi_3}-\frac{\partial x_p}{\partial \xi_3}\frac{\partial x_q}{\partial \xi_3}\frac{\partial f_j}{\partial \xi_2}\right)=-S_{1j}\frac{\partial f_1}{\partial \xi_3}.$$

Thus the term in $\frac{\partial}{\partial \xi_1}$ is reduced to

$$-\frac{\partial}{\partial \xi_1}\left(S_{1j}\frac{\partial f_1}{\partial \xi_k}\delta\xi_k\right).$$

Finally, with similar reductions of the terms in $\frac{\partial}{\partial \xi_2}$ and $\frac{\partial}{\partial \xi_3}$, we obtain

$$\frac{\partial}{\partial \xi_i}\left(\delta S_{ij}f_j\right)=-\frac{\partial}{\partial \xi_i}\left(S_{ij}\frac{\partial f_j}{\partial \xi_k}\delta\xi_k\right)=-\frac{\partial}{\partial \xi_i}\left(C_i\delta w^*\right)$$

as was to be proved.

8 Optimization Procedure

8.1 The Need for a Sobolev Inner Product in the Definition of the Gradient

Another key issue for successful implementation of the continuous adjoint method is the choice of an appropriate inner product for the definition of the gradient. It turns out that there is an enormous benefit from the use of a modified Sobolev gradient, which enables the generation of a sequence of smooth shapes. This can be illustrated by considering the simplest case of a problem in the calculus of variations.

Suppose that we wish to find the path $y(x)$ which minimizes

$$I=\int_a^b F(y,y')dx$$

with fixed end points $y(a)$ and $y(b)$. Under a variation $\delta y(x)$,

$$\begin{aligned}\delta I&=\int_a^b\left(\frac{\partial F}{\partial y}\delta y+\frac{\partial F}{\partial y'}\delta y'\right)dx\\&=\int_a^b\left(\frac{\partial F}{\partial y}-\frac{d}{dx}\frac{\partial F}{\partial y'}\right)\delta y dx\end{aligned}$$

Thus defining the gradient as

$$g=\frac{\partial F}{\partial y}-\frac{d}{dx}\frac{\partial F}{\partial y'}$$

and the inner product as

$$(u,v)=\int_a^b uvdx$$

we find that

$$\delta I=(g,\delta y).$$

If we now set

$$\delta y=-\lambda g,\qquad \lambda>0$$

we obtain a improvement

$$\delta I=-\lambda(g,g)\leq 0$$

unless $g=0$, the necessary condition for a minimum.

Note that g is a function of y,y',y'',

$$g=g(y,y',y'')$$

In the well known case of the Brachistrone problem, for example, which calls for the determination of the path of quickest descent

between two laterally separated points when a particle falls under gravity,

$$F(y,y') = \sqrt{\frac{1+y'^2}{y}}$$

and

$$g = -\frac{1+y'^2+2yy''}{2\left(y(1+y'^2)\right)^{3/2}}$$

It can be seen that each step

$$y^{n+1} = y^n - \lambda^n g^n$$

reduces the smoothness of y by two classes. Thus the computed trajectory becomes less and less smooth, leading to instability.

In order to prevent this we can introduce a weighted Sobolev inner product [16]

$$\langle u,v\rangle = \int (uv + \varepsilon u'v')dx$$

where ε is a parameter that controls the weight of the derivatives. We now define a gradient $\overline{g}$ such that

$$\delta I = \langle \overline{g}, \delta y\rangle$$

Then we have

$$\begin{aligned}\delta I &= \int (\overline{g}\delta y + \varepsilon \overline{g}'\delta y')dx \\ &= \int (\overline{g} - \frac{\partial}{\partial x}\varepsilon\frac{\partial \overline{g}}{\partial x})\delta y dx \\ &= (g,\delta y)\end{aligned}$$

where

$$\overline{g} - \frac{\partial}{\partial x}\varepsilon\frac{\partial \overline{g}}{\partial x} = g$$

and $\overline{g} = 0$ at the end points. Thus $\overline{g}$ can be obtained from g by a smoothing equation. Now the step

$$y^{n+1} = y^n - \lambda^n \overline{g}^n$$

gives an improvement

$$\delta I = -\lambda^n \langle \overline{g}^n, \overline{g}^n\rangle$$

but y^{n+1} has the same smoothness as y^n, resulting in a stable process.

8.2 Sobolev Gradient for Shape Optimization

In applying control theory to aerodynamic shape optimization, the use of a Sobolev gradient is equally important for the preservation of the smoothness class of the redesigned surface. Accordingly, using the weighted Sobolev inner product defined above, we define a modified gradient $\bar{\mathcal{G}}$ such that

$$\delta I = < \bar{\mathcal{G}}, \delta \mathcal{F} > .$$

In the one dimensional case $\bar{\mathcal{G}}$ is obtained by solving the smoothing equation

$$\bar{\mathcal{G}} - \frac{\partial}{\partial \xi_1}\varepsilon\frac{\partial}{\partial \xi_1}\bar{\mathcal{G}} = \mathcal{G}. \tag{36}$$

In the multi-dimensional case the smoothing is applied in product form. Finally we set

$$\delta \mathcal{F} = -\lambda \bar{\mathcal{G}} \tag{37}$$

with the result that

$$\delta I = -\lambda < \bar{\mathcal{G}}, \bar{\mathcal{G}} > \quad < 0,$$

unless $\bar{\mathcal{G}} = 0$, and correspondingly $\mathcal{G} = 0$.

When second-order central differencing is applied to (36), the equation at a given node, i, can be expressed as

$$\bar{\mathcal{G}}_i - \varepsilon\left(\bar{\mathcal{G}}_{i+1} - 2\bar{\mathcal{G}}_i + \bar{\mathcal{G}}_{i-1}\right) = \mathcal{G}_i, \qquad 1 \le i \le n,$$

where $\mathcal{G}_i$ and $\bar{\mathcal{G}}_i$ are the point gradients at node i before and after the smoothing respectively, and n is the number of design variables equal to the number of mesh points in this case. Then,

$$\bar{\mathcal{G}} = A\mathcal{G},$$

where A is the $n \times n$ tri-diagonal matrix such that

$$A^{-1} = \begin{bmatrix} 1+2\varepsilon & -\varepsilon & 0 & . & 0 \\ \varepsilon & . & . & & \\ 0 & . & . & . & \\ . & & . & . & -\varepsilon \\ 0 & & & \varepsilon & 1+2\varepsilon \end{bmatrix}.$$

Using the steepest descent method in each design iteration, a step, $\delta\mathcal{F}$, is taken such that

$$\delta\mathcal{F} = -\lambda A\mathcal{G}. \tag{38}$$

As can be seen from the form of this expression, implicit smoothing may be regarded as a preconditioner which allows the use of much larger steps for the search procedure and leads to a large reduction in the number of design iterations needed for convergence.

8.3 Outline of the Design Procedure

The design procedure can finally be summarized as follows:

1. Solve the flow equations for ρ, u_1, u_2, u_3, p.
2. Solve the adjoint equations for ψ subject to appropriate boundary conditions.
3. Evaluate $\mathcal{G}$ and calculate the corresponding Sobolev gradient $\bar{\mathcal{G}}$.
4. Project $\bar{\mathcal{G}}$ into an allowable subspace that satisfies any geometric constraints.
5. Update the shape based on the direction of steepest descent.
6. Return to 1 until convergence is reached.

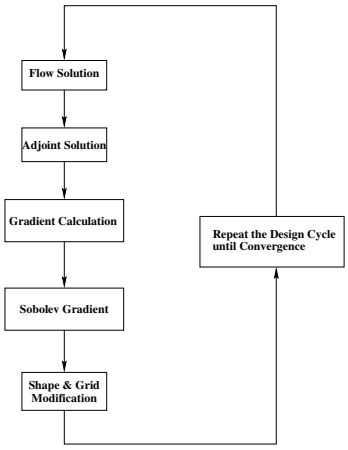

Figure 3. Design cycle

Practical implementation of the design method relies heavily upon fast and accurate solvers for both the state (w) and co-state (ψ) systems. The result obtained in Section 9 have been obtained using well-validated software for the solution of the Euler and Navier-Stokes equations developed over the course of many years [17–19]. For inverse design the lift is fixed by the target pressure. In drag minimization it is also appropriate to fix the lift coefficient, because the induced drag is a major fraction of the total drag, and this could be reduced simply by reducing the lift. Therefore the angle of attack is adjusted during each flow solution to force a specified lift coefficient to be attained, and the influence of variations of the angle of attack is included in the calculation of the gradient. The vortex drag also depends on the span loading, which may be constrained by other considerations such as structural loading or buffet onset. Consequently, the option is provided to force the span loading by adjusting the twist distribution as well as the angle of attack during the flow solution.

8.4 Computational Costs

In order to address the issues of the search costs, the authors investigated a variety of techniques in Reference [20] using a trajectory optimization problem (the brachistochrone) as a representative model. The study verified that the search cost (i.e., number of steps) of a simple steepest descent method applied to this problem scales as N^2, where N is the number of design variables, while the cost of quasi-Newton methods scaled linearly with N as expected. On the other hand, with an appropriate amount of smoothing, the smoothed descent method converged in a fixed number of steps, independent of N. Considering that the evaluation of the gradient by a finite difference method requires $N+1$ flow calculations, while the cost of its evaluation by the adjoint method is roughly that of two flow calculations, one arrives at the estimates of total computational cost given in Tables 1-2.

Table 1. Cost of Search Algorithm.

Steepest Descent	$O(N^2)$ steps
Quasi-Newton	$O(N)$ steps
Smoothed Gradient	$O(K)$ steps
(Note: K is independent of N)	

Table 2. Total Computational Cost of Design.

Finite Difference Gradients + Steepest Descent	$O(N^3)$
Finite Difference Gradients + Quasi-Newton Search	$O(N^2)$
Adjoint Gradients + Quasi-Newton Search	$O(N)$
Adjoint Gradients + Smoothed Gradient Search (Note: K is independent of N)	$O(K)$

9 Case Studies

Several design efforts which have utilized these methods include: Raytheon's and Gulfstream business jets, NASA's High-Speed Civil Transport, regional jet designs, as well as several Boeing projects such as the MDXX and the Blended-Wing-Body [21, 22]. Some representation examples of design calculations are presented in this section to illustrate the present capability.

9.1 Redesign of the Boeing 747 wing

Over the last decade the adjoint method has been successfully used to refine a variety of designs for flight at both transonic and supersonic cruising speeds. In the case of transonic flight, it is often possible to produce a shock free flow which eliminates the shock drag by making very small changes, typically no larger than the boundary layer displacement thickness. Consequently viscous effects need to be considered in order to realize the full benefits of the optimization.

Here the optimization of the wing of the Boeing 747-200 is presented to illustrate the kind of benefits that can be obtained. In these calculations the flow was modeled by the Reynolds Averaged Navier-Stokes equations. A Baldwin Lomax turbulence model was considered sufficient, since the optimization is for the cruise condition with attached flow. The calculation were performed to minimize the drag coefficient at a fixed lift coefficient, subject to the additional constraints that the span loading should not be altered and the thickness should not be reduced. It might be possible to reduce the induced drag by modifying the span loading to an elliptic distribution, but this would increase the root bending moment, and consequently require an increase in the skin thickness and structure weight. A reduction in wing thickness would not only reduce the fuel volume, but it would also require an increase in skin thickness to support the bending moment. Thus these constraints assure that there will be no penalty in either structure weight or fuel volume.

Figure 6 displays the result of an optimization at a Mach number of 0.86, which is roughly the maximum cruising Mach number attainable by the existing design before the onset of significant drag rise. The lift coefficient of 0.42 is the contribution of the exposed wing. Allowing for the fuselage to total lift coefficient is about 0.47. It can be seen that the redesigned wing is essentially shock free, and the drag coefficient is reduced from 0.01269 (127 counts) to 0.01136 (114 counts). The total drag coefficient of the aircraft at this lift coefficient is around 270 counts, so this would represent a drag reduction of the order of 5 percent.

Figure 7 displays the result of an optimization at Mach 0.90. In this case the shock waves are not eliminated, but their strength is significantly weakened, while the drag coefficient is reduced from 0.01819 (182 counts) to 0.01293 (129 counts). Thus the redesigned wing has essentially the same drag at Mach 0.9 as the original wing at Mach 0.86. The Boeing 747 wing could apparently be modified to allow such an increase in the cruising Mach number because it has a higher sweep-back than later designs, and a rather thin wing section with a thickness to chord ratio of 8 percent. Figures 8 and 9 verify that the span loading and thickness were not changed by the redesign, while figures 10 and 11 indicate the required section changes at 42 percent and 68 percent span stations.

9.2 Planform and Aero-structural Optimization

The shape changes in the section needed to improve the transonic wing design are quite small. However, in order to obtain a true optimum design larger scale changes such as changes in the wing planform (sweepback, span, chord, and taper) should be considered. Because these directly affect the structure weight, a meaningful result can only be obtained by considering a cost function that takes account of both the aerodynamic characteristics and the weight.

In references [23–25] the cost function is defined as

$$I = \alpha_1 C_D + \alpha_2 \frac{1}{2} \int_{\mathcal{B}} (p - p_d)^2 dS + \alpha_3 C_W$$

where C_W is a dimensionless measure of the wing weight, which can be estimated either from statistical formulas, or from a simple analysis of a representative structure, allowing for failure modes such as panel buckling. The coefficient α_2 is introduced to provide the designer some control over the pressure distribution, while the relative importance of drag and weight are represented by the coefficients α_1 and α_3. By varying these it is possible to calculate the Pareto front of designs which have the least weight for a given drag coefficient, or the least drag coefficient for a given weight. The relative importance of these can be estimated from the Breguet range equation (1).

Figure 28 shows the Pareto front obtained from a study of the Boeing 747 wing [25], in which both the wing planform and section were varied simultaneously, with the planform defined by five parameters; sweepback, span, and the chord at three span stations. In this case the planform variations were limited to changes in sweepback, and the section changes were constrained to maintain the same thickness to chord ratio. When $\frac{\alpha_3}{\alpha_1}$ is relatively large, the optimum wing has a reduced sweepback, leading to a weight reduction, as illustrated in figure 29. The accompanying section shape changes keep the shock drag low.

Figure 28 also shows the point on the front that is estimated to produce the maximum range according to the Breguet equation.

9.3 Wing inverse design using an unstructured mesh

A major obstacle to the treatment of arbitrarily complex configurations is the difficulty and cost of mesh generation. This can

be mitigated by the use of unstructured meshes. Thus it appears that the extension of the adjoint method to unstructured meshes may provide the most promising route to the optimum shape design of key elements of complex configurations, such as wing-pylon-nacelle combinations. Some results are presented below. These have been obtained with new software to implement the adjoint method for unstructured meshes which is currently under development [26]. Figures 12 and 13 shows the result of an inverse design calculation, where the initial geometry was a wing made up of NACA 0012 sections and the target pressure distribution was the pressure distribution over the Onera M6 wing. Figures 14, 15, 16, 17, 18, 19, show the target and computed pressure distribution at six span-wise sections. It can be seen from these plots the target pressure distribution is well recovered in 50 design cycles, verifying that the design process is capable of recovering pressure distributions that are significantly different from the initial distribution. This is a particularly challenging test, because it calls for the recovery of a smooth symmetric profile from an asymmetric pressure distribution containing a triangular pattern of shock waves.

9.4 Shape optimization for a Transonic Business Jet

The unstructured design method has also been applied to complete aircraft configurations. The results for a business jet are shown below. As shown in figures 20, 21, 22, 23, the outboard sections of the wing have a strong shock while flying at cruise conditions ($M_\infty = 0.80$, $\alpha = 2^o$). The results of a drag minimization that aims to remove the shocks on the wing are shown in figures 24, 25, 26, 27. The drag has been reduced from 235 counts to 215 counts in about 8 design cycles. The lift was constrained at 0.4 by perturbing the angle of attack. Further, the original thickness of the wing was maintained during the design process ensuring that fuel volume and structural integrity will be maintained by the redesigned shape. Thickness constraints on the wing were imposed on cutting planes along the span of the wing and by transferring the constrained shape movement back to the nodes of the surface triangulation. The volume mesh was deformed to conform to the shape changes induced using the spring method. The entire design process typically takes about 4 hours on a 1.7 Ghz Athlon processor with 1 Gb of memory. Parallel implementation of the design procedure has also been developed that further reduces the computational cost of this design process.

10 Conclusion

The accumulated experience of the last decade suggests that most existing aircraft which cruise at transonic speeds are amenable to a drag reduction of the order of 3 to 5 percent, or an increase in the drag rise Mach number of at least .02. These improvements can be achieved by very small shape modifications, which are too subtle to allow their determination by trial and error methods. The potential economic benefits are substantial, considering the fuel costs of the entire airline fleet. Moreover, if one were to take full advantage of the increase in the lift to drag ratio during the design process, a smaller aircraft could be designed to perform the same task, with consequent further cost reductions. It seems inevitable that some method of this type will provide a basis for aerodynamic designs of the future.

Acknowledgment

This work has benefited greatly from the support of the Air Force Office of Science Research under grant No. AF F49620-98-1-2002. I have drawn extensively from the lecture notes prepared by Luigi Martinelli and myself for a CIME summer course in 1999 [14] and from a paper prepared for the 23^{rd} International Congress of Aeronautical Sciences, Toronto, September 2002 [27]. I am also indebted to my research assistant Kasidit Leoviriyakit for his assistance in preparing the Latex files for this text.

REFERENCES

[1] M. Van Dyke. *An Album of Fluid Motion*. The Parabolic Press, Stanford, 1982.

[2] D.R. Chapman, H. Mark, and M.W. Pirtle. Computers vs. wind tunnels in aerodynamic flow simulations. *Astronautics and Aeronautics*, 13(4):22–30, 35, 1975.

[3] Levy D.W., Zickuhr T., Vassberg J., and al. Summary of data from the first aiaa cfd drag prediction workshop. *AIAA paper 02-0841*, AIAA 40rd Aerospace Sciences Meeting, Reno, Nevada, January 2002.

[4] G. Redeker. DLR-F4 wing-body configuration. In *A Selection of Experimental Test Cases for the Validation of CFD Codes*, number *AR-303*, pages B4.1–B4.21. AGARD, August 1994.

[5] J. Vassberg, P.G. Buning, and C.L. Rumsey. Drag prediction for the dlr-f4 wing/body using overflow and cfl3d on an overset mesh. *AIAA paper 02-0840*, AIAA 40rd Aerospace Sciences Meeting, Reno, Nevada, January 2002.

[6] R. M. Hicks and P. A. Henne. Wing design by numerical optimization. *Journal of Aircraft*, 15:407–412, 1978.

[7] C. Bischof, A. Carle, G. Corliss, A. Griewank, and P. Hovland. Generating derivative codes from Fortran programs. *Internal report MCS-P263-0991*, Computer Science Division, Argonne National Laboratory and Center of Research on Parallel Computation, Rice University, 1991.

[8] L. L. Green, P. A. Newman, and K. J. Haigler. Sensitivity derivatives for advanced CFD algorithm and viscous modeling parameters via automatic differentiation. *AIAA paper 93-3321*, 11th AIAA Computational Fluid Dynamics Conference, Orlando, Florida, 1993.

[9] W. K. Anderson, J. C. Newman, D. L. Whitfield, and E. J. Nielsen. Sensitivity analysis for the Navier-Stokes equations on unstructured meshes using complex variables. *AIAA paper 99-3294*, Norfolk, VA, June 1999.

[10] A. Jameson, L. Martinelli, J. J. Alonso, J. C. Vassberg, and J. Reuther. Simulation based aerodynamic design. *IEEE Aerospace Conference*, Big Sky, MO, March 2000.

[11] A. Jameson. Optimum aerodynamic design using control theory. *Computational Fluid Dynamics Review*, pages 495–528, 1995.

[12] A. Jameson. Optimum aerodynamic design using CFD and control theory. *AIAA paper 95-1729*, AIAA 12th Computational Fluid Dynamics Conference, San Diego, CA, June 1995.

[13] A. Jameson, L. Martinelli, and N. A. Pierce. Optimum aerodynamic design using the Navier-Stokes equations. *Theoret. Comput. Fluid Dynamics*, 10:213–237, 1998.

[14] A. Jameson and L. Martinelli. Aerodynamic shape optimization techniques based on control theory. Lecture notes in mathematics #1739, proceeding of computational mathematics driven by industrial problems, CIME (International Mathematical Summer (Center), Martina Franca, Italy, June 21-27 1999.

[15] A. Jameson. Aerodynamic shape optimization using the adjoint method. 2002-2003 lecture series at the von karman institute, Von Karman Institute For Fluid Dynamics, Brussels, Belgium, Febuary 3-7 2003.

[16] A. Jameson, L. Martinelli, and J. Vassberg. Reduction of the adjoint gradient formula in the continuous limit. *AIAA paper*, 41^{st} AIAA Aerospace Sciences Meeting, Reno, NV, January 2003.

[17] A. Jameson, W. Schmidt, and E. Turkel. Numerical solutions of the Euler equations by finite volume methods with Runge-Kutta time stepping schemes. *AIAA paper 81-1259*, January 1981.

[18] L. Martinelli and A. Jameson. Validation of a multigrid method for the Reynolds averaged equations. *AIAA paper 88-0414*, 1988.

[19] S. Tatsumi, L. Martinelli, and A. Jameson. A new high resolution scheme for compressible viscous flows with shocks. *AIAA paper* To Appear, AIAA 33nd Aerospace Sciences Meeting, Reno, Nevada, January 1995.

[20] A. Jameson and J. C. Vassberg. Studies of alternative numerical optimization methods applied to the brachistochrone problem. In *Proceedings of OptiCON'99*, Newport Beach, CA, October 1999.

[21] R. H. Liebeck. Design of the Blended-Wing-Body subsonic transport. *Wright Brothers Lecture, AIAA paper 2002-0002*, Reno, NV, January 2002.

[22] D. L. Roman, J. B. Allen, and R. H. Liebeck. Aerodynamic design challenges of the Blended-Wing-Body subsonic transport. *AIAA paper 2000-4335*, Denver, CO, August 2000.

[23] K. Leoviriyakit and A. Jameson. Aerodynamic shape optimization of wings including planform variations. *AIAA paper 2003-0210*, 41^{st} Aerospace Sciences Meeting & Exhibit, Reno, Nevada, January 2003.

[24] K. Leoviriyakit, S. Kim, and A. Jameson. Viscous aerodynamic shape optimization of wings including planform variables. *AIAA paper 2003-3498*, 21^{st} Applied Aerodynamics Conference, Orlando, Florida, June 23-26 2003.

[25] K. Leoviriyakit and A. Jameson. Aero-structural wing planform optimization. Reno, Nevada, January 2004. Proceedings of the 42^{st} Aerospace Sciences Meeting & Exhibit.

[26] A. Jameson, Sriram, and L. Martinelli. An unstructured adjoint method for transonic flows. *AIAA paper*, 16^{th} AIAA CFD Conference, Orlando, FL, June 2003.

[27] A. Jameson. Using computational fluid dynamics for aerodynamics - a critical assessment. Technical report, 23^{rd} International Congress of Aeronautical Sciences, Toronto, Canada, September 8-13 2002.

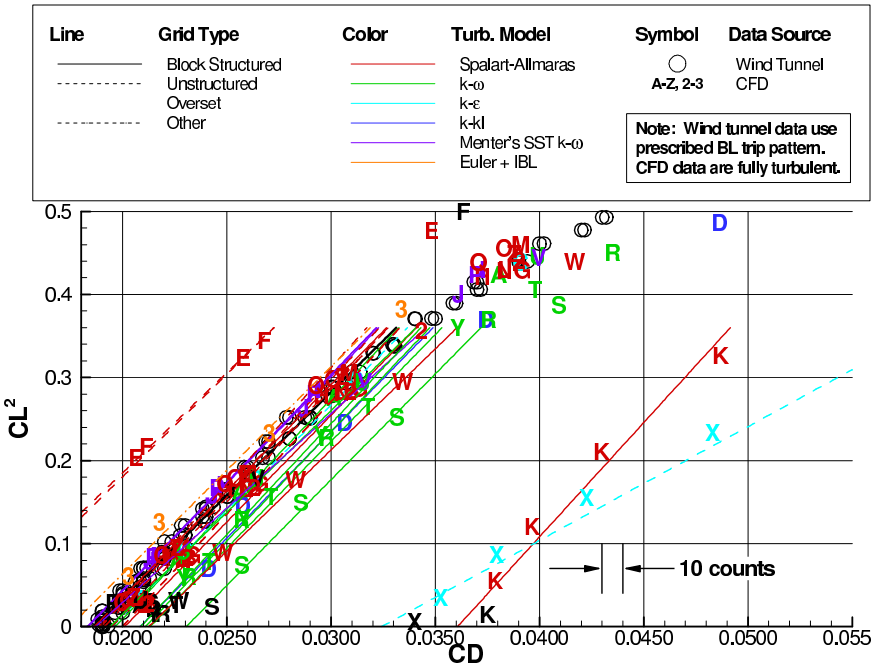

Figure 4. Composite Drag Results form Reference [3]

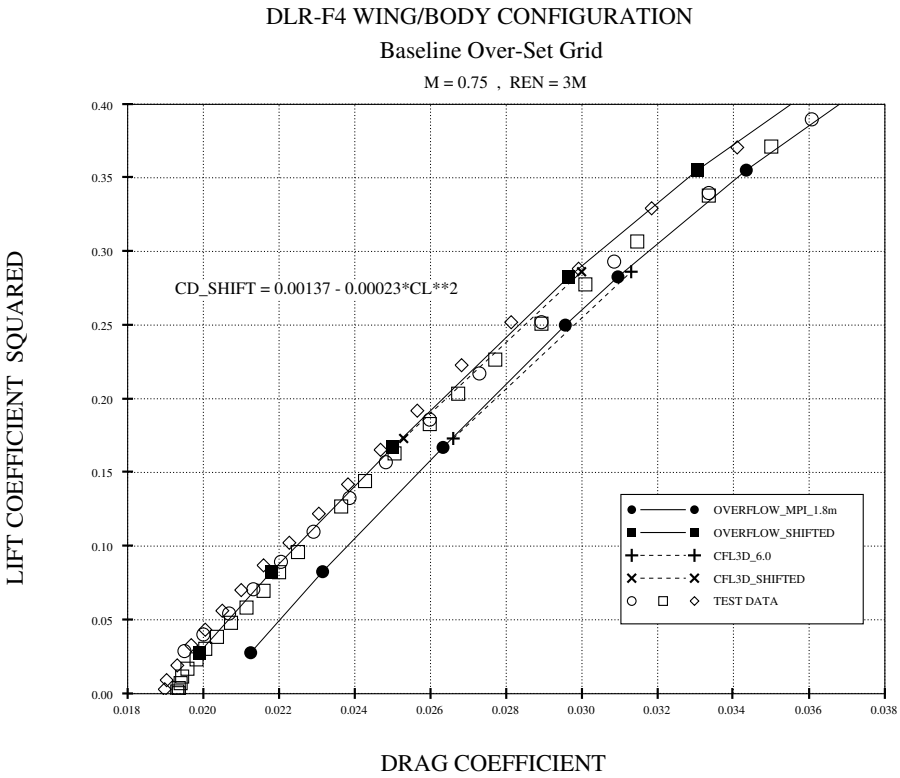

Figure 5. OVERFLOW Drag Polars with and without Transition Corrections.

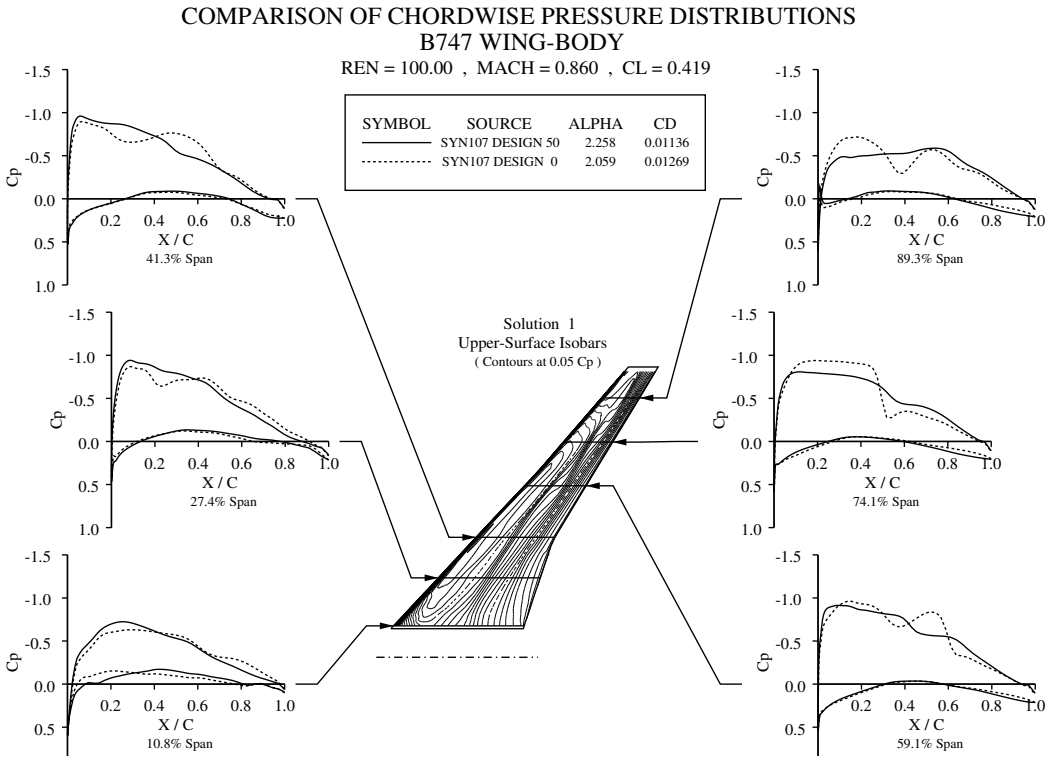

Figure 6. Redesigned Boeing 747 wing at Mach 0.86, Cp distributions

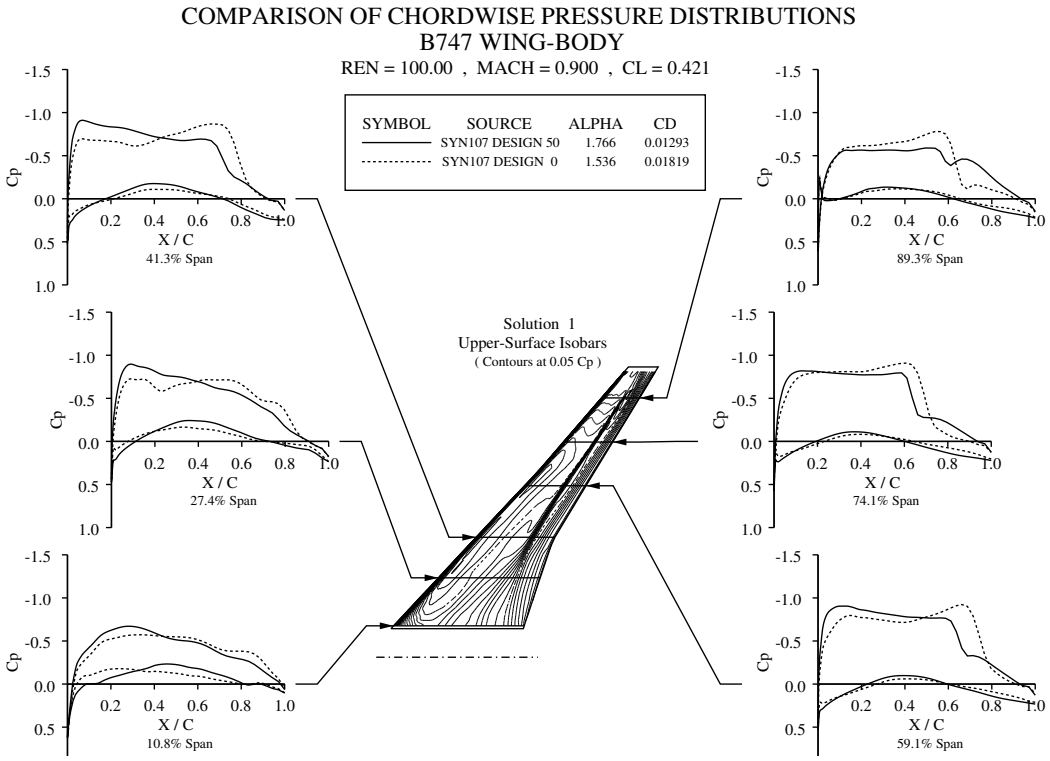

Figure 7. Redesigned Boeing 747 wing at Mach 0.90, Cp distributions

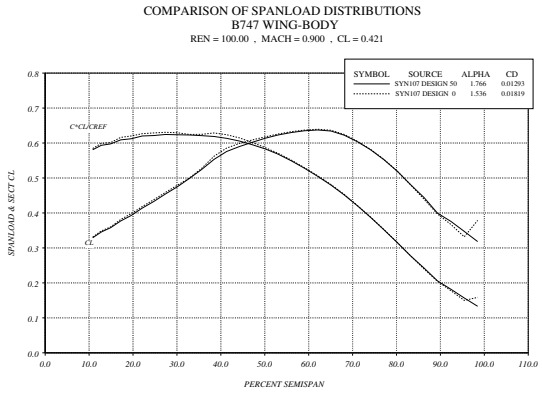

Figure 8. Span loading, Redesigned Boeing 747 wing at Mach 0.90

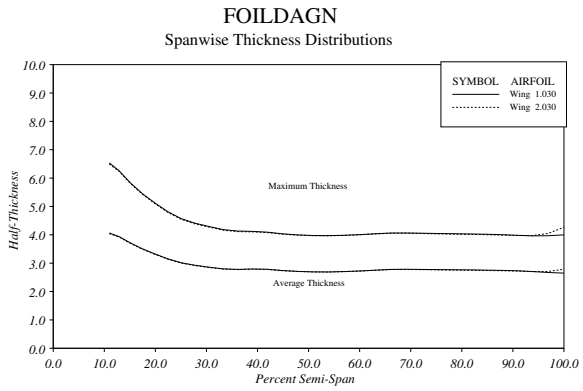

Figure 9. Spanwise thickness distribution, Redesigned Boeing 747 wing at Mach 0.90

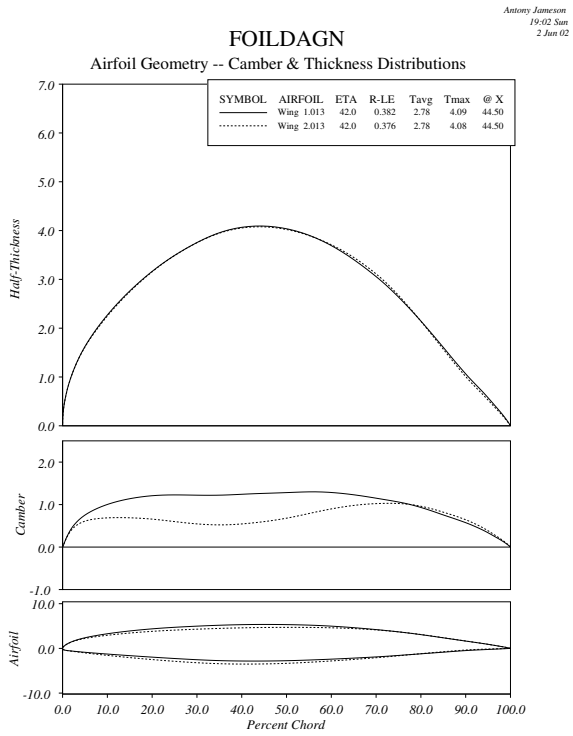

Figure 10. Section geometry at η = 0.42, redesigned Boeing 747 wing at Mach 0.90

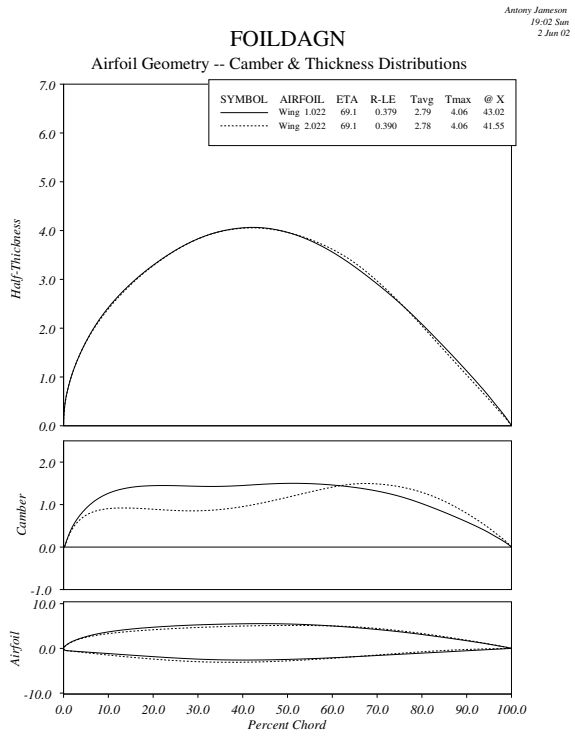

Figure 11. Section geometry at η = 0.68, redesigned Boeing 747 wing at Mach 0.90

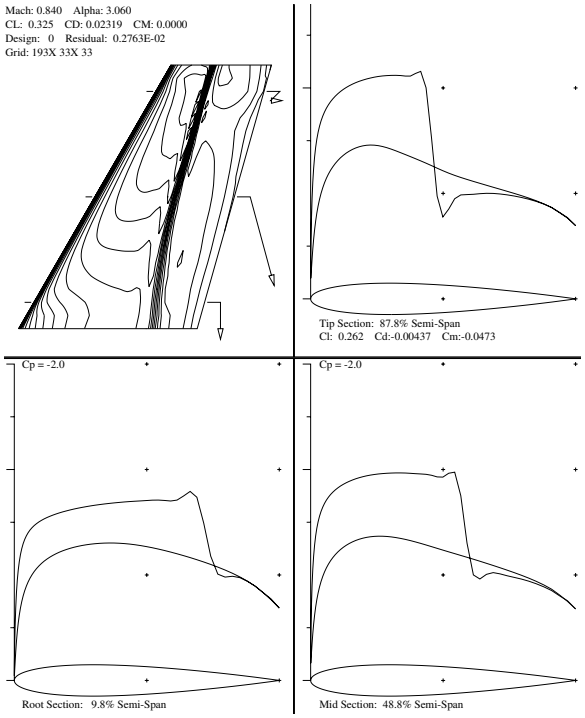

Figure 12. Initial(dashed lines) and final (solid lines) over a NACA 0012 wing

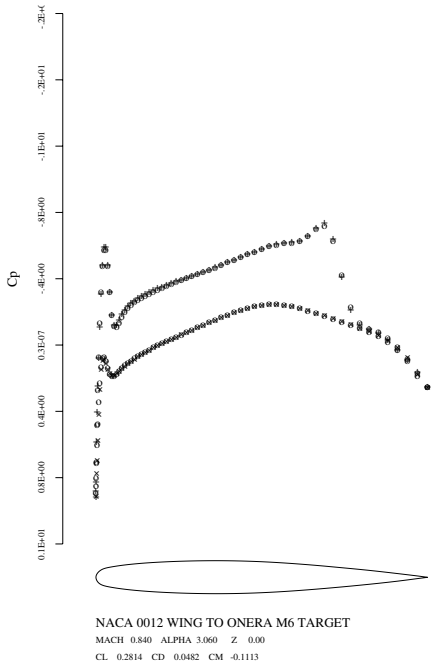

Figure 14. Attained(+,x) and target(o) pressure distributions at 0 % of the wing span

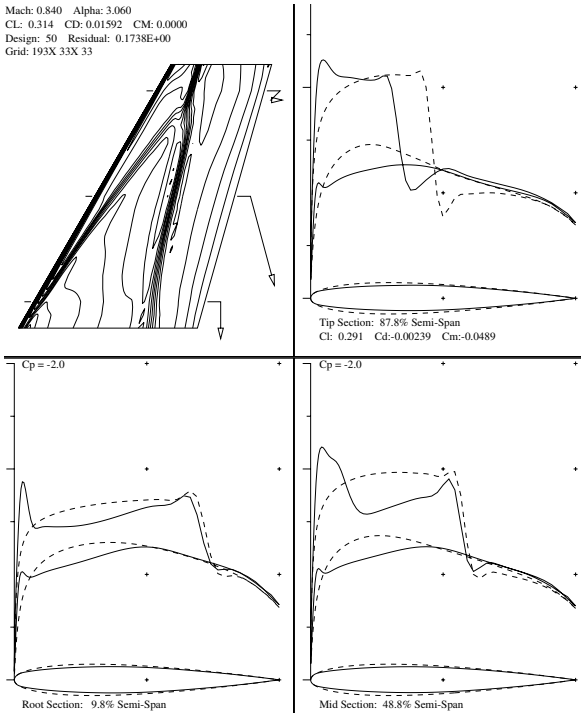

Figure 13. Initial(dashed lines) and final (solid lines) pressure distribution and modified section geometries

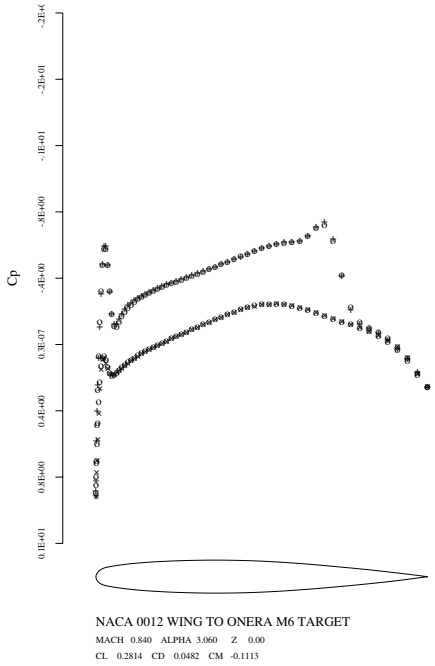

Figure 15. Attained(+,x) and target(o) pressure distributions at 20 % of the wing span

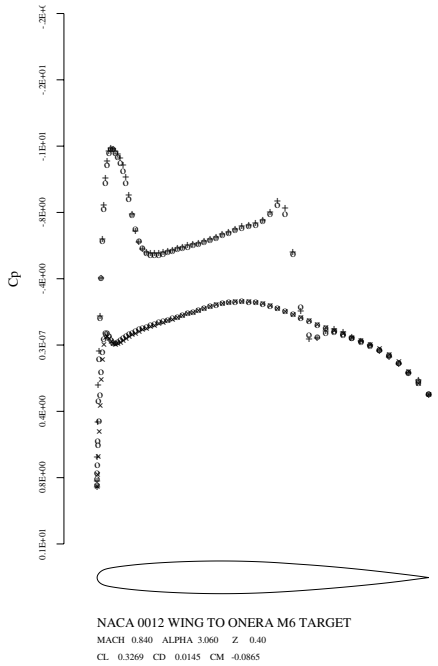

Figure 16. Attained(+,x) and target(o) pressure distributions at 40 % of the wing span

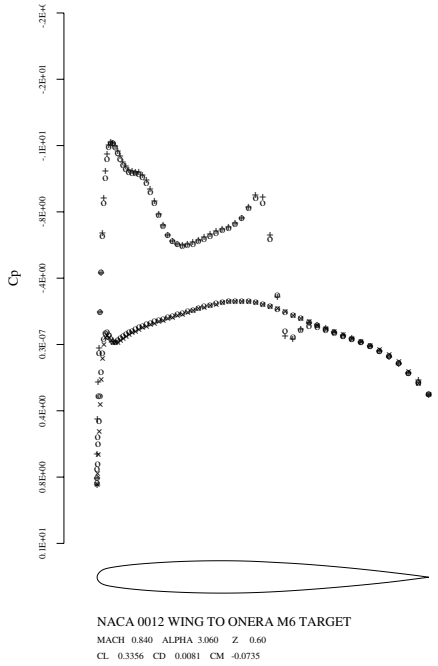

Figure 17. Attained(+,x) and target(o) pressure distributions at 60 % of the wing span

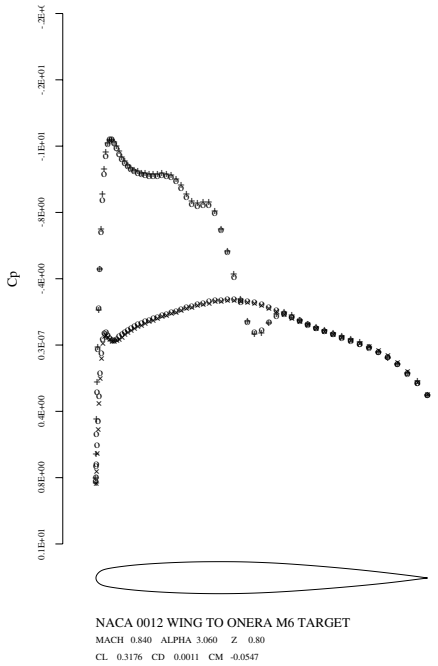

Figure 18. Attained(+,x) and target(o) pressure distributions at 80 % of the wing span

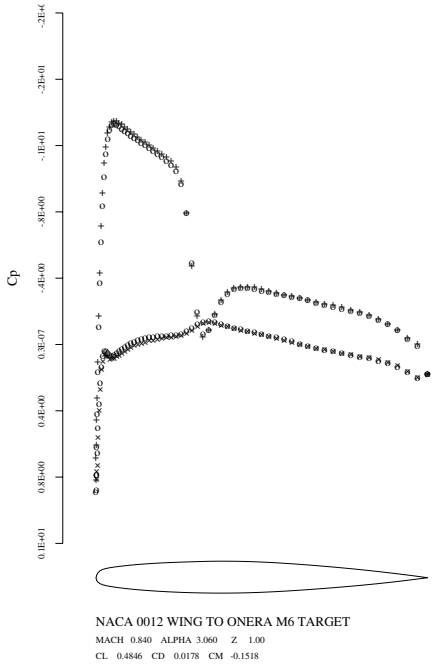

Figure 19. Final computed and target pressure distributions at 100 % of the wing span

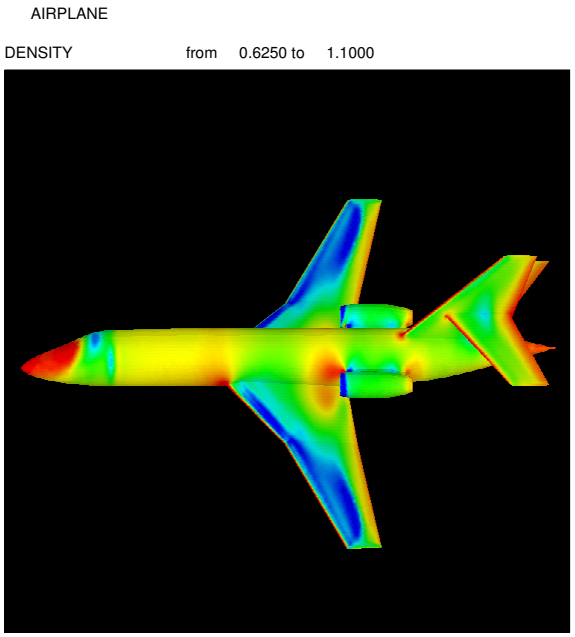

Figure 20. Density contours for a business jet at $M = 0.8, \alpha = 2$

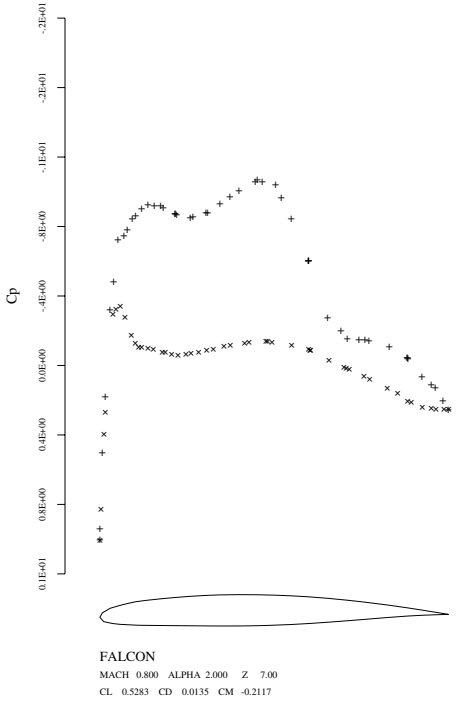

Figure 22. Pressure distribution at 77 % wing span

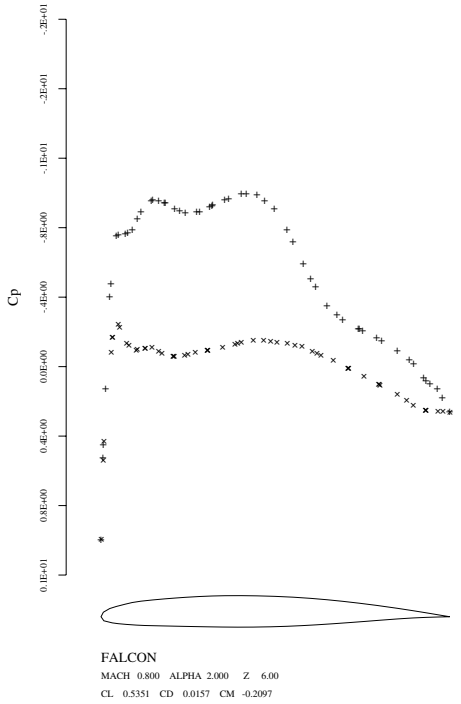

Figure 21. Pressure distribution at 66 % wing span

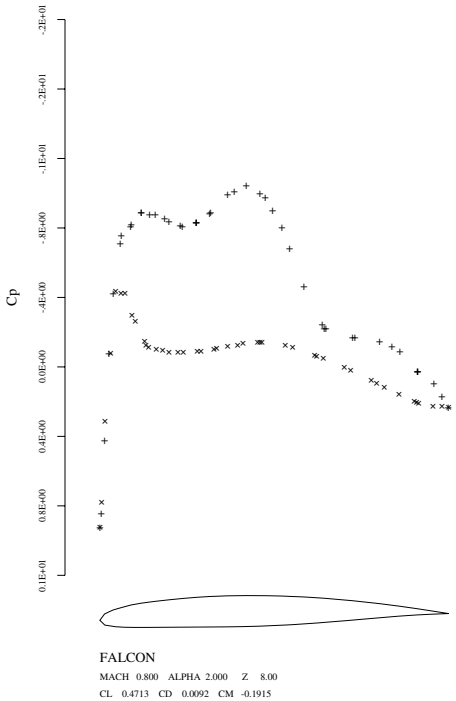

Figure 23. Pressure distribution at 88 % wing span

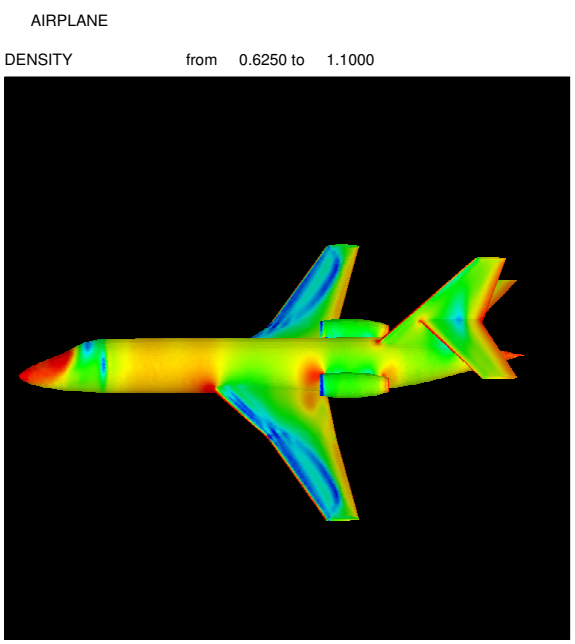

Figure 24. Density contours for a business jet at $M = 0.8$, $\alpha = 2.3$, after redesign

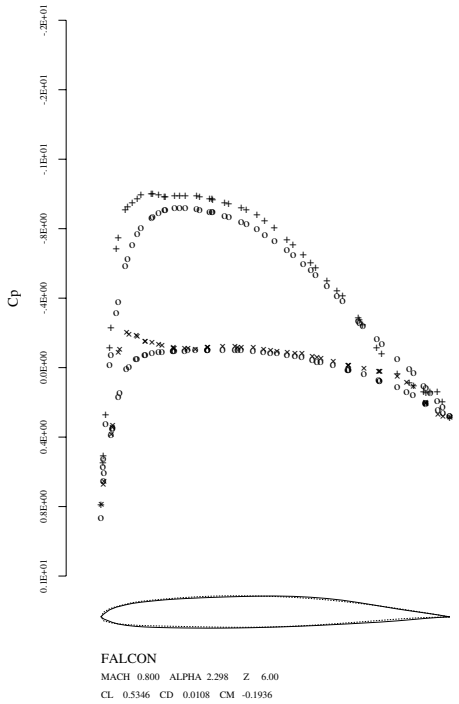

Figure 25. Pressure distribution at 66 % wing span, after redesign, Dashed line: original geometry, solid line: redesigned geometry

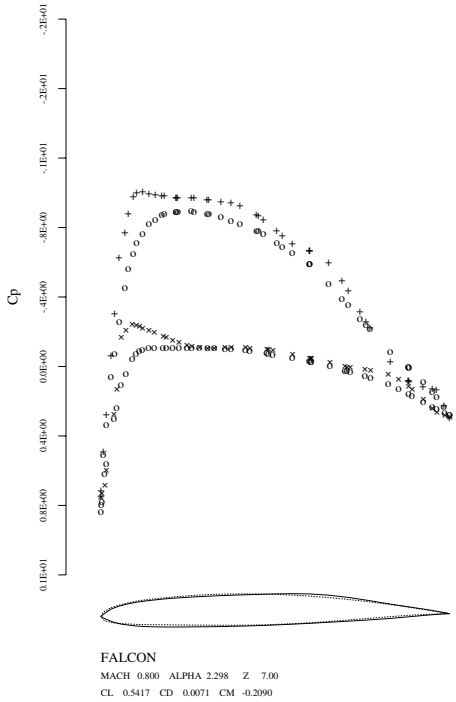

Figure 26. Pressure distribution at 77 % wing span, after redesign, Dashed line: original geometry, solid line: redesigned geometry

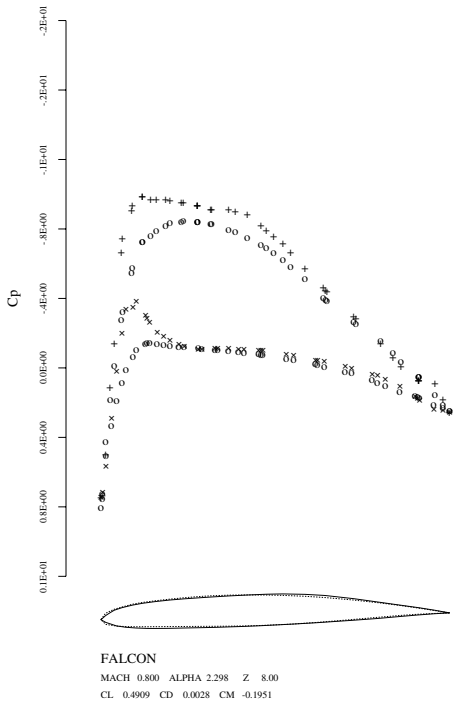

Figure 27. Pressure distribution at 88 % wing span, after redesign, Dashed line: original geometry, solid line: redesigned geometry

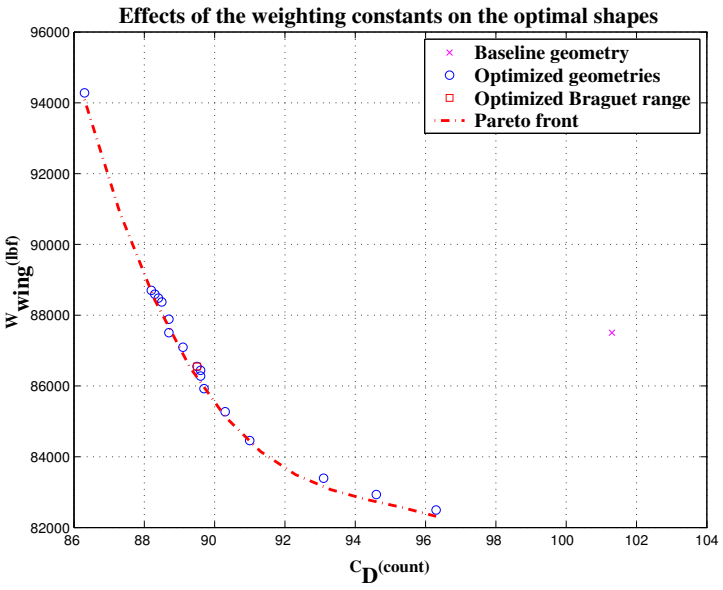

Figure 28. Pareto front of section and sweep modifications

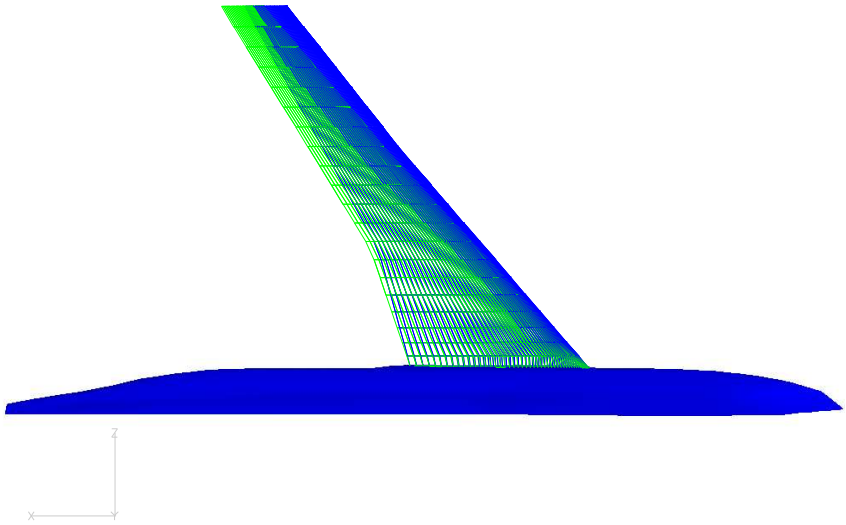

Figure 29. Superposition of the baseline geometry (green) and the optimized planform geometry (blue), using α_1=1 and α_3=0.5.